AIAA JOURNAL
Vol. 45, No. 8, August 2007

Suppression of Thermal Postbuckling and Nonlinear Panel Flutter Motions Using Piezoelectric Actuators

Qinqin Li,* Chuh Mei,† and Jen-Kuang Huang‡
Old Dominion University, Norfolk, Virginia 23529

DOI: 10.2514/1.28280

Active output feedback control of large amplitude nonlinear panel flutter at supersonic speeds with and without temperature effect is presented. A coupled structural-electrical modal formulation using finite elements is applied. Suppression of three types of panel response is studied: limit cycle oscillations, static thermal postbuckling, and chaotic motion. The controller, composed of a linear quadratic regulator and an extended Kalman filter, is developed and investigated. The extended Kalman filter considers the nonlinear state-space matrix and has a gain sequence evaluated online. The norms of the feedback control gain are employed for the optimal placement of piezoelectric actuators, and the norms of the Kalman filter estimation gain are used to validate the best locations for the sensors. A symmetric laminated composite plate at supersonic speeds with or without the influence of elevated temperatures is investigated. Two types of piezoelectric materials, PZT5A and macrofiber composite actuators, embedded in the composite panel are considered to suppress the nonlinear panel flutter. Simulation results show that the linear quadratic regulator/Kalman filter controller can suppress all three types of panel response with or without thermal effects.

Nomenclature

$\bar{\mathbf{A}}$, $\mathbf{B}$, $\mathbf{C}$, $\mathbf{D}$	=	system state-space matrices
$\hat{\mathbf{A}}$, $\hat{\mathbf{B}}$, $\hat{\mathbf{C}}$, $\hat{\mathbf{D}}$	=	observer state-space matrices
$[A]$	=	system aerodynamic influence matrix
e_c	=	error between desired panel deflection and observer output
e_i	=	error between analytical and observer model of the panel
F	=	state transition matrix
$[G]$, $[\bar{G}]$	=	system and modal aerodynamic damping matrices
h	=	beam or composite plate thickness
J	=	cost functional
K, K_e	=	optimal control and estimate gain matrix
$[K]$, $[K_{\text{lin}}]$, $[\bar{K}]$	=	system, combined system, and modal stiffness matrices
$[K1]$, $[K2]$	=	combined system first- and second-order nonlinear stiffness matrices
$[\bar{K}_{qq}]$	=	modal nonlinear stiffness matrix
$[M]$, $[\bar{M}]$	=	system and modal mass matrices
$\{\boldsymbol{P}_{\boldsymbol{\Delta T}}\}$	=	thermal load vector
Q	=	state weighting matrix
Q_e, R_e	=	covariance matrices
$\{\boldsymbol{q}\}$	=	natural modal coordinate vector
R	=	control effort weighting matrix
U	=	control input
u	=	system input (compensator output)
$\{\boldsymbol{w}\}$, $\{\boldsymbol{W}\}$	=	element and system nodal displacement vectors
$\boldsymbol{X}$, $\hat{\boldsymbol{X}}$	=	state and estimated state vectors
$\boldsymbol{Y}$, $\hat{\boldsymbol{Y}}$	=	sensor output and estimated output vectors
y, $\hat{y}$	=	system real and estimated outputs
ΔT	=	thermal
$\{\boldsymbol{\varepsilon}\}$	=	strain vector
λ	=	nondimensional dynamic pressure
ρ, ρ_p	=	mass densities
ϕ	=	fiber orientation angle
ω	=	frequency

Received 9 October 2006; revision received 15 February 2007; accepted for publication 15 February 2007.

*Research Assistant, Department of Aerospace Engineering.
†Professor, Department of Aerospace Engineering. Associate Fellow AIAA.
‡Professor, Department of Mechanical Engineering. Member AIAA.

I. Introduction

AT SUPERSONIC environment, high-speed vehicles may endure severe aerodynamic pressure and thermal loads. Panel flutter is one phenomenon caused by airflow acting on one side of the skin panels of the vehicle. When the dynamic pressure is above the critical value, the panel motion exhibits bounded limit cycle oscillations (LCO), and the amplitude of the LCO increase as the dynamic pressure increases. At elevated temperatures, the panel even undergoes thermal postbuckling deflection (but dynamically stable) or chaotic motions. All of these three types of panel response, LCO, thermal postbuckling, and chaos, are considered for suppression in this paper.

The review of nonlinear panel flutter by Mei et al. [1] listed that the optimal control, the rate feedback control, and the active compensation of aerodynamic stiffness control are the main active control methods to suppress the linear and nonlinear panel flutter. Most of those control studies have successfully controlled LCO without thermal influences. Considering thermal effects, optimal control of LCO has been discussed by Zhou et al. [2,3]. Moon and Kim [4] suppressed the LCO under thermal effects with active/passive hybrid piezoelectric networks. Park and Kim [5] applied macrofiber composite (MFC) actuators [6,7] to passively suppress the nonlinear panel flutter under uniform temperature distribution. They showed that in-plane actuation of the MFC can increase the critical temperature and the critical dynamic pressure, and decrease the large thermal deflection. Recently, Moon et al. [8] proposed a full-state feedback linearization controller to suppress the LCO of panel flutter under sinusoidal thermal loads. As a nonlinear controller designed based on a nonlinear model, it can enlarge the range of the maximum suppressible dynamic pressure $\lambda_{\max}$ compared with linear controllers or controllers designed based on linear models. However, all states might not be available in practical situations, and a nonlinear estimator may be useful. Furthermore, active suppression of static thermal postbuckling and chaotic motions under thermal environments are seldom discussed in the literature in this field.

Recently, Li et al. [9] used an active output feedback controller consisting of a linear quadratic regulator (LQR) and an extended Kalman filter (EKF) [10,11] to provide adaptive control of nonlinear free vibrations of composite plates using piezoelectric actuators. The experience gained in [9] is extended to use of this controller to suppress the nonlinear panel flutter because panel flutter is a self-excited dynamic behavior. The coupled structural-electrical nonlinear modal equations of motion using the finite elements are based on the von Karman nonlinear strain-displacement relations, the linear piezoelectricity constitution equations, the classic laminated composite plate theory, and the first-order quasi-steady aerodynamic piston theory. For the first time, this paper presents the suppression of all three nonlinear flutter responses at elevated temperatures, LCO (including periodic motions), thermal postbuckling deflection, and chaotic motions. Two types of piezoelectric actuators and sensors are employed: PZT5A and MFC. They were placed on the panel via the norms of the feedback control gain (NFCG) and the norms of the Kalman filter estimation gain (NKFEG) method [2,3,9]. Successful suppression results with time responses will be shown later.

II. System Modeling

A. Fundamental Theories

Dowell [12] has classified the panel flutter into four categories by considering the linearity or nonlinearity in structures and aerodynamics, and four approaches for flutter analysis. The four analysis methods include Galerkin's method [13,14], harmonic balance method, finite element method [1,15], and perturbation method. In this work, the finite element method is applied to model the flutter behavior and investigate the flutter suppression.

The advantages of this approach are that a model of the system can use von Karman [16] nonlinear strain-stress relations, a linear piezoelectricity constitution equation, and classic laminated composite theory together, and still provide accurate results when compared with other methods [1]. In addition, the finite element method can model with ease [7] both the traditional monolithic isotropic piezoceramic wafers (PZT5A) and the high-performance directional or anisotropic MFC. The most significant result, from a control point of view, is that by applying a modal transformation to a finite element model of a system, the size of the system can be reduced to an order of four or six modes. This reduced-base model makes it much easier for controller design.

To analyze and control the response of panel flutter at supersonic speeds, quasi-steady first-order piston aerodynamic theory is applied [1,12,14]. A finite element model of the rectangular plates was built based on the Bogner–Fox–Schmit element [17].

B. System Equations

The derivation of the equations of motion for nonlinear panel flutter at elevated temperatures can be found in [5,8,18–21]. After assembling the element matrices and applying the kinematical boundary conditions in standard finite element procedure, the system equations of motion for an isotropic or symmetrically laminated composite plate at supersonic speeds and uniformly distributed temperatures can be expressed as follows:

$$\begin{bmatrix}[M] & 0\\ 0 & 0\end{bmatrix}\begin{Bmatrix}\ddot{\boldsymbol{W}}\\ \ddot{\boldsymbol{W}}_\phi\end{Bmatrix}+\begin{bmatrix}[G] & 0\\ 0 & 0\end{bmatrix}\begin{Bmatrix}\dot{\boldsymbol{W}}\\ \dot{\boldsymbol{W}}_\phi\end{Bmatrix}+\left(\begin{bmatrix}[K_w] & [K_{w\phi}]\\ [K_{\phi w}] & [K_\phi]\end{bmatrix}+\begin{bmatrix}[K_1] & 0\\ 0 & 0\end{bmatrix}+\begin{bmatrix}[K_2] & 0\\ 0 & 0\end{bmatrix}+\lambda\begin{bmatrix}[A] & 0\\ 0 & 0\end{bmatrix}-\begin{bmatrix}[K_{\Delta T}] & 0\\ 0 & 0\end{bmatrix}\right)\begin{Bmatrix}\boldsymbol{W}\\ \boldsymbol{W}_\phi\end{Bmatrix}=\begin{Bmatrix}\{\boldsymbol{P_{\Delta T}}\}\\ 0\end{Bmatrix} \tag{1}$$

where

$$[M]=\begin{bmatrix}[M_b] & 0\\ 0 & 0\end{bmatrix},\qquad [G]=\begin{bmatrix}[G_a(\lambda, C_a)] & 0\\ 0 & 0\end{bmatrix}$$

$$[A]=\begin{bmatrix}[A_a] & 0\\ 0 & 0\end{bmatrix},\qquad [K_w]=\begin{bmatrix}[K_b] & 0\\ 0 & [K_m]\end{bmatrix}$$

$$[K_{\Delta T}]=\begin{bmatrix}[K_{\Delta Tb}] & 0\\ 0 & 0\end{bmatrix},\qquad [K_{w\phi}]=\begin{bmatrix}[K_{b\phi}]\\ 0\end{bmatrix}=[K_{\phi w}]^T$$

$$[K_1]=\begin{bmatrix}[K1_{Nm}] & [K1_{bm}]\\ [K1_{mb}] & 0\end{bmatrix}$$

$$[K_2]=\begin{bmatrix}[K2_b] & 0\\ 0 & 0\end{bmatrix},\quad \text{and}\quad \{\boldsymbol{P_{\Delta T}}\}=\begin{bmatrix}0\\ \{\boldsymbol{P_{\Delta T}}_m\}\end{bmatrix}$$

In Eq. (1), $[K_w]$ is the linear stiffness matrix, and$[K_{\Delta T}]$ is a stiffness matrix due the thermal load. The structural node displacement vector $\{\boldsymbol{W}\}=\{\boldsymbol{W}_b, \boldsymbol{W}_m\}^T$ is the combination of bending and in-plane displacements [18,19], and $\{\boldsymbol{W}_\phi\}=\{V_1,\ldots,V_k,\ldots,V_{np}\}^T$ is the electric degree of freedom (DOF) in which V_k denotes the electric voltage applied to the kth piezoelectric layer. Matrix $[G_a]$ is the aerodynamic damping, $[A_a]$ is the aerodynamic influence, and $\lambda=2q_a a^3/D_{110}(M_\infty^1-1)^{1/2}$ is a nondimensional dynamic pressure, in which q_a is the dynamic pressure, a is the plate length, D_{110} is the first entry of the laminate bending stiffness matrix $[D]$ determined with all fibers of the composite layers in the x direction as a reference, and M_∞ is the Mach number.

A combination of the value of λ and temperature ratio $(\Delta T/\Delta T_{\text{cr}})$ will determine what kind of panel flutter response (flat, buckled, LCO, periodic but not harmonic, and chaotic motion) can be expected [1,18]. Governing equations for the PZT/MFC actuators and sensors embedded in the composite panel are expressed by $\{\boldsymbol{W}_\phi\}$ DOF [2–5,7,9,20]

$$\{\boldsymbol{W}_\phi\}=\begin{Bmatrix}\boldsymbol{W}_\phi^a\\ \boldsymbol{W}_\phi^s\end{Bmatrix} \tag{2}$$

The remaining matrices from Eq. (1) also need to be written as

$$[K_{\phi w}]=\begin{bmatrix}[K_{\phi w}^a]\\ [K_{\phi w}^s]\end{bmatrix}=[K_{w\phi}]^T\quad\text{and}\quad [K_\phi]=\begin{bmatrix}[K_\phi^a] & 0\\ 0 & [K_\phi^s]\end{bmatrix} \tag{3}$$

Thus, Eq. (1) can be written as two equations:

$$[M]\{\ddot{\boldsymbol{W}}\}+[G]\{\dot{\boldsymbol{W}}\}+([K_{\text{lin}}]+[K_1]+[K_2])\{\boldsymbol{W}\}=\{\boldsymbol{P_{\Delta T}}\}-[K_{w\phi}]\{\boldsymbol{W}_\phi\} \tag{4}$$

$$[K_{\phi w}]\{\boldsymbol{W}\}=-[K_\phi]\{\boldsymbol{W}_\phi\} \tag{5}$$

where $[K_{\text{lin}}]$ can be expressed as

$$[K_{\text{lin}}]=[K_w]+\lambda[A]-[K_{\Delta T}] \tag{6}$$

Considering Eq. (5) as a sensor equation first

$$\{q^s\}=\left[K_\phi^s\right]\left\{W_\phi^s\right\}=-\left[K_{\phi w}^s\right]\{W\} \tag{7}$$

Since $\{W_\phi^s\}$ is the sensor voltage and $[K_\phi^s]$ is regarded as a capacitance here, $\{q^s\}$ represents the electric charge. The output of the system is given by the charge of the sensor, and the actuator equation can be derived from it,

$$\{q^a\}=\left[K_\phi^a\right]\left\{\boldsymbol{W}_\phi^a\right\}=-\left[K_{\phi w}^a\right]\{\boldsymbol{W}\} \tag{8}$$

Similarly $\{q^a\}$ means actuator charge which is not of interest, and so Eq. (8) is ignored. Then Eq. (4) is considered. It gives the relationship between the actuator voltage, sensor voltage, and the deflection.

$$[M]\{\ddot{\boldsymbol{W}}\}+[G]\{\dot{\boldsymbol{W}}\}+([K_{\text{lin}}]+[K_1]+[K_2])\{\boldsymbol{W}\}=\{\boldsymbol{P_{\Delta T}}\}-\left[K_{w\phi}^s\right]\left\{\boldsymbol{W}_\phi^s\right\}-\left[K_{w\phi}^a\right]\left\{\boldsymbol{W}_\phi^a\right\} \tag{9}$$

Because the actuator voltage is much larger than the sensor voltage, Eq. (9) can be reduced to

$$[M]\{\ddot{\boldsymbol{W}}\} + [G]\{\dot{\boldsymbol{W}}\} + ([K_{\text{lin}}] + [K_1] + [K_2])\{\boldsymbol{W}\} = \{\boldsymbol{P_{AT}}\} - \left[K^a_{w\phi}\right]\left\{\boldsymbol{W}^a_{\phi}\right\} \tag{10}$$

From Eq. (1), the actuator and sensor equations become

$$[M_b]\{\ddot{\boldsymbol{W}}_b\} + [G_a]\{\dot{\boldsymbol{W}}_b\} + ([K] + [K2])\{\boldsymbol{W}_b\} = -\left[K^a_{b\phi}\right]\left\{\boldsymbol{W}^a_{\phi}\right\} \tag{11}$$

$$\{q^s\} = \left[K^s_{\phi b}\right]\left\{\boldsymbol{W}^s_{\phi}\right\} = -\left[K^s_{\phi b}\right]\{\boldsymbol{W}_b\} \tag{12}$$

where the matrices $[K]$ and $[K2]$ can be expressed as

$$[K] = [K_b] + \lambda[A_a] + [K_{\Delta Tb}] + [K_{Nm}(\{\boldsymbol{W}_m\}_0)] \tag{13}$$

$$[K2] = [K2_b] - [K1_{bm}][K_m]^{-1}[K1_{mb}] - [K1_{Nm}(\{\boldsymbol{W}_m\}_2)] \tag{14}$$

$$\{\boldsymbol{W}_m\}_0 = -[K_m]^{-1}\{\boldsymbol{P_{m\Delta T}}\} \tag{15}$$

$$\{\boldsymbol{W}_m\}_2 = -[K_m]^{-1}[K1_{mb}]\{\boldsymbol{W}_b\} \tag{16}$$

Self-sensing actuators are simultaneously actuators and sensors. This means $\{\boldsymbol{W}_\phi\}$, $[K_{w\phi}]$, $[K_{\phi w}]$, and $[K_\phi]$ are not separated into two parts [20,21]. Then, the equations of motion for self-sensing actuators are

$$[M_b]\{\ddot{W}_b\} + [G_a]\{\dot{\boldsymbol{W}}_b\} + ([K] + [K2])\{\boldsymbol{W}_b\} = -[K_{b\phi}]\{\boldsymbol{W}_\phi\} \tag{17}$$

$$\{q^s\} = -[K_{b\phi}]\{\boldsymbol{W}_b\} \tag{18}$$

C. Modal Equations

For a set of modal equations, there is no need to assemble and update the nonlinear stiffness matrix at each time integration step, and the number of modal equations is much smaller than the structure DOF equations [18,20,21]. A modal transformation can be applied to obtain the system modal equations of motion. The panel deflection can be expressed as a linear combination of some known function as

$$\{\boldsymbol{W}_b\} = \sum_{r=1}^{n} q_r(t)\{\psi_r\} = [\Phi]\{\boldsymbol{q}\} \tag{19}$$

The linear frequencies and corresponding natural modes are obtained from the linear vibration of the system

$$\omega_r^2[M_b]\{\psi_r\} = [K_b]\{\psi_r\} \tag{20}$$

If tracing back to element matrices of the system [9,18], the element nonlinear stiffness matrices can be expressed by the element displacements, in turn, they can be expressed by the linear modes $\{\psi_r\}$. Thus, the actuation equations of motion in modal coordinates become:

$$[\bar{M}_b]\{\ddot{\boldsymbol{q}}\} + [\bar{G}]\{\dot{\boldsymbol{q}}\} + ([\bar{K}] + [\bar{K}_{qq}])\{\boldsymbol{q}\} = -[\bar{K}_{b\phi}]\{\boldsymbol{W}_\phi\} \tag{21}$$

and the sensing modal equation is

$$\{\boldsymbol{q}^s\} = -[\bar{K}_{\phi b}]\{\boldsymbol{q}\} \tag{22}$$

A modal piezoelectric control force is defined as follows:

$$[\bar{K}_{b\phi}] = [\Phi]^T[K_{b\phi}] = [\bar{K}_{\phi b}]^T \tag{23}$$

The second-order nonlinear modal stiffness matrix in Eq. (20) is shown by

$$[\bar{K}_{qq}] = [\Phi]^T \sum_{r=1}^{n}\sum_{s=1}^{n} q_r q_s([K2_b]^{rs} + [K2_{Nm}]^{rs} - [K1_{bm}]^r[K_m]^{-1}[K1_{mb}]^s)[\Phi] \tag{24}$$

Then, after defining all components of the stiffness matrix in the preceding equations, the modal mass, linear stiffness, and aerodynamic damping matrices can be put together in compact notation:

$$([\bar{M}_b], [\bar{K}], [\bar{G}]) = [\Phi]^T([M_b], [K], [G(\lambda, C_a)])[\Phi] \tag{25}$$

The modes that are included in the response analysis can be determined [20,21] from the modal participation value for the rth mode

$$(\max|q_r|)/(\sum_{s=1}^{n}\max|q_s|)$$

It was investigated [1,13,18] that nonlinear panel flutter in modal formulation achieves sufficient convergence when the contributions of the first four modes are taken into consideration.

D. Placement of Sensors and Actuators

The placement of sensors and actuators is another important factor in the suppression of nonlinear flutter. Optimal locations for placement of the sensors and actuators could make the control very effective. On the other hand, poorly chosen locations may degrade the control results and even produce a spillover of the system. Here, the NFCG and NKFEG methods are used to select the optimal locations for both actuators and sensors, respectively. The NFCG norm method [2,3,9,20] performs a sum of the square of the LQR gain for every element, and can be calculated when an actuator is placed at each element of the object with

$$\text{NFCG} = \sqrt{\sum_{j=1}^{2n} k_{ij}^2}, \qquad (i = 1, 2, \ldots, N) \tag{26}$$

where k_{ij} is the element of the feedback gain K obtained for LQR, $2n$ is the total number of state variables defined later in Eq. (31), and N is the number of piezoelectric actuator sets. If the value for this location is higher, it has more control authority at this location. When each NFCG norm is calculated for each location, locations with a higher NFCG norm are chosen to be the optimal locations for actuators. Similarly, the optimal sensor locations can be chosen by the Kalman filter feedback estimation gain [9,20]:

$$\text{NKFEG} = \sqrt{\sum_{j=1}^{2n} ke_{ij}^2}, \qquad (i = 1, 2, \ldots, N) \tag{27}$$

where ke_{ij} is the element of the feedback gain K_e from an EKF filter. The higher the value for this location, the more sensing ability the value has for this location. When each NKFEG norm is calculated for each location, locations with a higher NKFEG norm are chosen to be the optimal locations for the sensors.

Sensor placement solutions for different plate models are presented in Figs. A1–A4 in the Appendix. It is shown that in all cases the same tendency can be observed for the PZT5A and the MFC: they should be placed close to the edges of the plate for optimal performance.

III. Controller Design

The compensator used in this study is the output feedback controller composed of an linear quadratic regulator and an extended Kalman filter. The EKF includes the nonlinear part of the model and can give an accurate estimation of the states of a system. The LQR controller was chosen due to its flexibility in design, especially for multivariable systems (in this case a multimodes system).

Table 1 Material property of the composite plate, PZT5A, and MFC

Materials	Graphite-epoxy	PZT5A	MFC
Young's modulus, psi	$E_1 = 22.50 \cdot 10^6$	$E_p = 9.00 \cdot 10^6$	$E_{p1} = 5.29 \cdot 10^6$
N/m^2	$15.5 \cdot 10^{10}$	$6.21 \cdot 10^{10}$	$6.51 \cdot 10^{10}$
	$E_2 = 1.17 \cdot 10^6$	——	$E_{p2} = 1.10 \cdot 10^6$
	$8.07 \cdot 10^9$	——	$7.58 \cdot 10^9$
Shear modulus, psi	$G_{12} = 0.66 \cdot 10^6$	$G_p = 3.46 \cdot 10^6$	$G_{p12} = 2.12 \cdot 10^6$
N/m^2	$4.55 \cdot 10^9$	$2.39 \cdot 10^{10}$	$1.46 \cdot 10^{10}$
	——	——	$G_{p23} = 1.06 \cdot 10^6$
	——	——	$7.31 \cdot 10^9$
Poisson's ratio	$\nu_1 = 0.22$	——	$\nu_{p1} = 0.25$
	$\nu_2 = 0.011$	$\nu = 0.30$	$\nu_{p2} = 0.05$
Density, $lb \cdot s^2/in.^4$	$\rho = 1.458 \cdot 10^{-4}$	$\rho_p = 7.10 \cdot 10^{-4}$	$\rho_{p23} = 7.07 \cdot 10^{-4}$
kg/m^3	1550	7582	7552
Thickness, in.	$h = 0.054$	$h = 0.009$	$h = 0.009$
m	$1.37 \cdot 10^{-3}$	$2.3 \cdot 10^{-4}$	$2.3 \cdot 10^{-4}$
Charge constant, in./V	——	$d_{31} = -7.51 \cdot 10^{-9}$	$d_{11} = 2.09 \cdot 10^{-8}$
m/V	——	$-1.91 \cdot 10^{-10}$	$5.31 \cdot 10^{-10}$
	——	——	$d_{12} = -8.27 \cdot 10^{-9}$
	——	——	$-2.10 \cdot 10^{-10}$
Electrode space, in.	——	$h_k = 0.009$	$h_k = 0.042$
m	——	$2.3 \cdot 10^{-4}$	$1.07 \cdot 10^{-3}$
Maximum voltage, V	——	$V_{\max} = 820$	$V_{\max} = 2000$

A. System State-Space Model

Based on the modal equations of motion, Eqs. (21) and (22), a standard state-space model for control design and simulation can be formed. The system state vector $\boldsymbol{X}$ consists of the modal amplitudes and velocities

$$\boldsymbol{X} = \begin{Bmatrix} q \\ \dot{q} \end{Bmatrix} \tag{28}$$

and as defined in the nomenclature, the control input and the sensor input are

$$U = \{\boldsymbol{W}_\phi\} \tag{29}$$

$$\boldsymbol{Y} = \{q^s\} \tag{30}$$

The state-space form for the modal equations of motion is then

$$\dot{\boldsymbol{X}} = \bar{\mathbf{A}}\boldsymbol{X} + \mathbf{B}U \qquad \boldsymbol{Y} = \mathbf{C}\boldsymbol{X} + \mathbf{D}U \tag{31}$$

where the system matrices are

$$\bar{\mathbf{A}} = \begin{bmatrix} 0 & I \\ -[\bar{M}_b]^{-1}[\bar{K}] & -[\bar{M}_b]^{-1}[\bar{G}] \end{bmatrix} + \begin{bmatrix} 0 & 0 \\ -[\bar{M}_b]^{-1}[\bar{K}_{qq}] & 0 \end{bmatrix}$$
$$\mathbf{B} = \begin{bmatrix} 0 \\ -[\bar{M}_b]^{-1}[\bar{K}_{b\phi}] \end{bmatrix} \qquad \mathbf{C} = \begin{bmatrix} -[\bar{K}_{\phi b}] & 0 \end{bmatrix} \qquad \mathbf{D} = 0 \tag{32}$$

and where $\bar{\mathbf{A}}$ is a real system state matrix. In designing a controller for the system, we use its linearization form by applying the Taylor series approach. In fact, the linearized $\mathbf{A}$ matrix is the first part of $\bar{\mathbf{A}}$

$$\mathbf{A} = \begin{bmatrix} 0 & I \\ -[\bar{M}_b]^{-1}[\bar{K}] & -[\bar{M}_b]^{-1}[\bar{G}] \end{bmatrix} \tag{33}$$

B. Linear Quadratic Regulator Control

Here, a linear quadratic regulator is used for our system. This method seeks a solution for the linear full-state feedback problem defined as

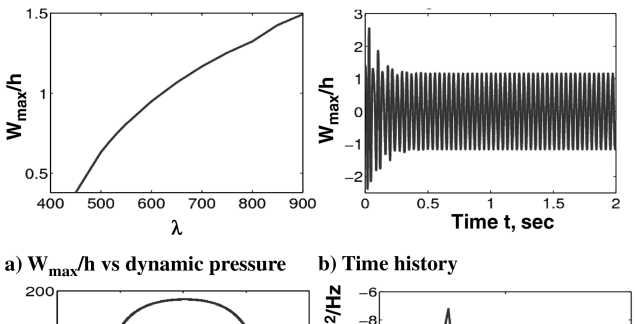

a) W_{max}/h vs dynamic pressure b) Time history

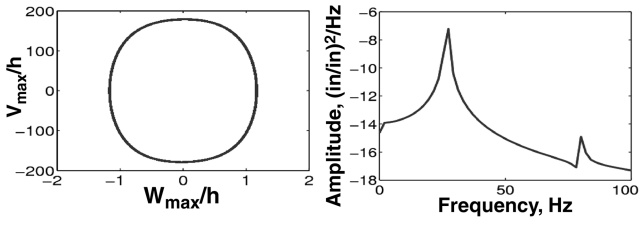

c) Phase plot d) Power spectrum density

Fig. 1 LCO response of the composite panel at $\lambda = 700$ using 4 modes.

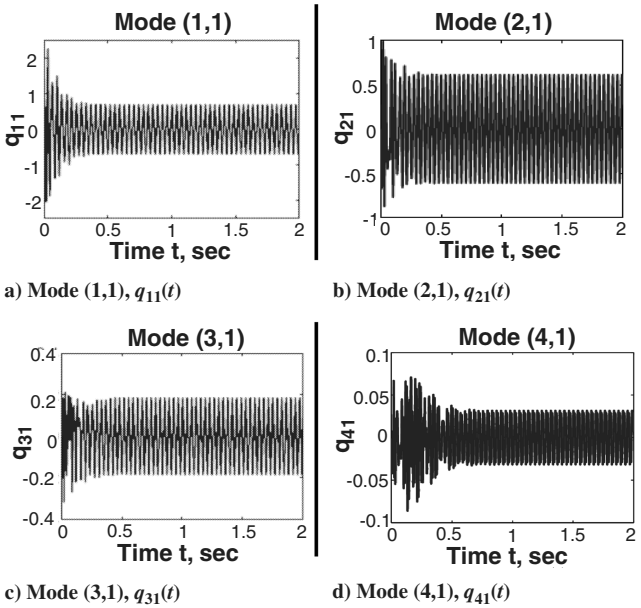

a) Mode (1,1), $q_{11}(t)$ b) Mode (2,1), $q_{21}(t)$

c) Mode (3,1), $q_{31}(t)$ d) Mode (4,1), $q_{41}(t)$

Fig. 2 Time histories of the 4 modes for the composite panel at $\lambda = 700$.

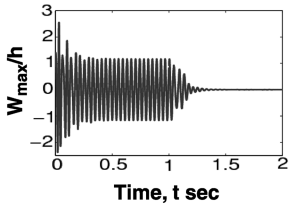

a) Controlled panel LCO

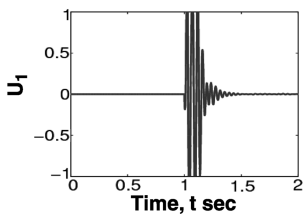

b) Control input 1

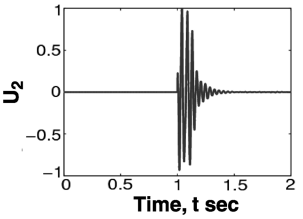

c) Control input 2

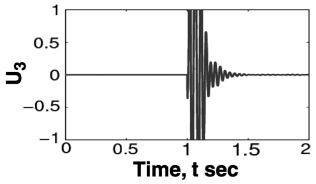

d) Control input 3

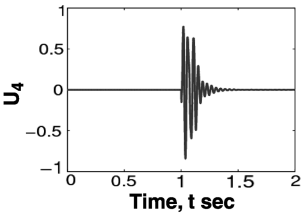

e) Control input 4

Fig. 3 Suppression of LCO at $\lambda = 700$ using PZT5A.

$$U = -KX \tag{34}$$

which minimizes a quadratic performance index that is a cost functional of system states and control effort

$$J = \int_0^\infty [X^T Q X + U^T R U]\,\mathrm{d}t \tag{35}$$

Minimizing Eq. (35), the controller gain is

$$K = R^{-1}\mathbf{B}^T P + Q = 0 \tag{36}$$

where P is a positive definite symmetric matrix determined from the

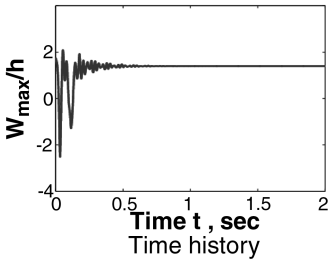

Fig. 5 Thermal postbuckling of the composite panel at $\lambda = 430$ and $\Delta T/\Delta T_{cr} = 8$ using 4 modes.

solution of the algebraic Riccati equation

$$\mathbf{A}^T P + P\mathbf{A} - P\mathbf{B}R^{-1}\mathbf{B}^T P + Q = 0 \tag{37}$$

To apply the LQR control, all the states of the system are to be known. In fact, it is difficult for the sensor to give the accurate information for every state. Thus, the state estimator needs to be used like the linear Kalman filter. Linearized system equations are used and nonlinear effects are not considered during the process. State estimation performance for large amplitude limit cycle amplitudes may be deteriorated as a result [21], and the extended Kalman filter [22] is thus implemented. It replaces the nominal trajectory based on the linearized system by the estimated trajectory, then evaluates the Taylor series about the estimated trajectory. Thus, if the system is sufficiently observable, the estimated trajectory is close to actual trajectory sufficiently and makes the estimation valid.

The nonlinear state estimation is

$$\dot{\hat{X}} = \bar{\mathbf{A}}(\hat{X}, t)\hat{X} + \mathbf{B}U + K_e(t)(Y - \mathbf{C}\hat{X}) \tag{38}$$

$$\hat{Y} = \mathbf{C}\hat{X} \tag{39}$$

The EKF contains the nonlinearity for the system dynamics, which is linearized according to the traditional Kalman filter, accounting for the better robustness of the extended Kalman filter. The EKF uses linear approximation over a very small range of the state space. Then, the Riccati equation is solved to get the EKF gains. In fact, in our system, the linear approximation is for every step of the iteration for a nonlinear system. The resulting linearization's range is much smaller

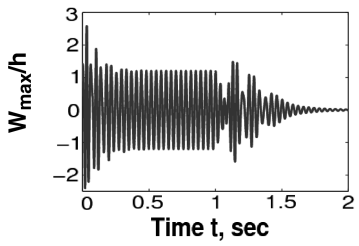

a) Controlled LCO

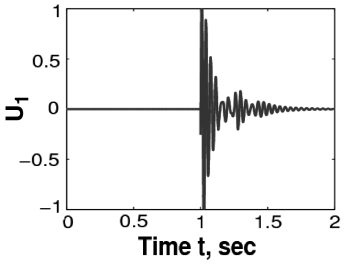

b) Controlled input 1

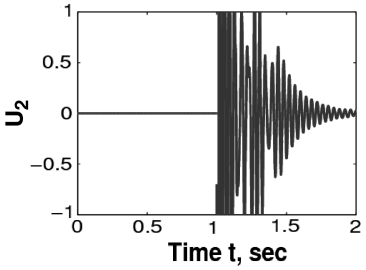

c) Controlled input 2

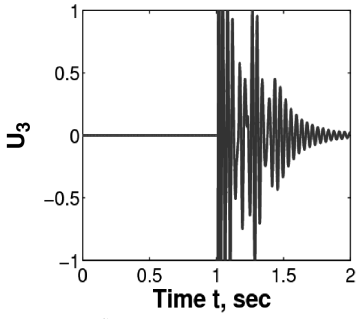

d) Controlled input 3

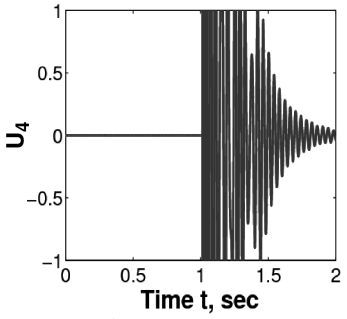

e) Controlled input 4

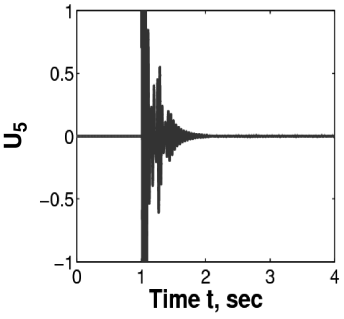

f) Controlled input 5

Fig. 4 Suppression of LCO at $\lambda = 700$ using MFC.

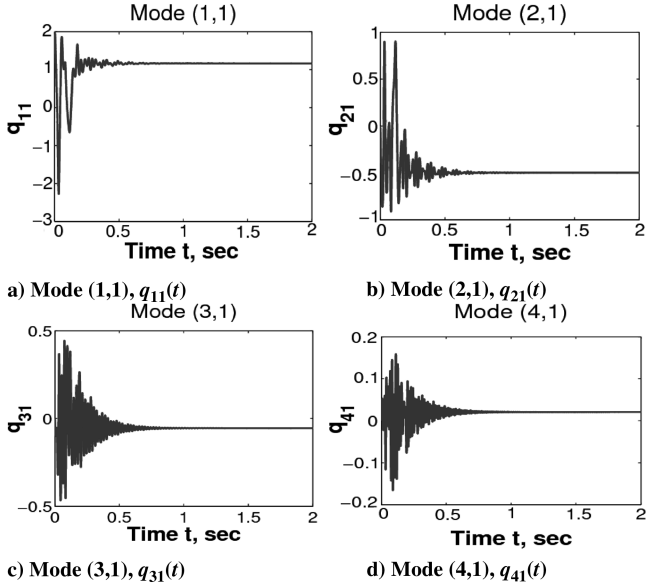

a) Mode (1,1), $q_{11}(t)$ b) Mode (2,1), $q_{21}(t)$

c) Mode (3,1), $q_{31}(t)$ d) Mode (4,1), $q_{41}(t)$

Fig. 6 Time histories of the 4 modes for the composite panel at $\lambda = 430$ and $\Delta T/\Delta T_{cr} = 8$.

than the linearization of the traditional Kalman filter (which is the same as the linearization for LQR). Thus, the EKF can have better state estimation.

The linear approximation of the state matrix (or the state transition matrix) is

$$F(t) \approx \left.\frac{\partial f(x,t)}{\partial x}\right|_{x=\hat{x}(t)} = \left.\begin{bmatrix} \frac{\partial f_1}{\partial x_1} & \frac{\partial f_1}{\partial x_2} & \frac{\partial f_1}{\partial x_3} & \cdots & \frac{\partial f_1}{\partial x_n} \\ \frac{\partial f_2}{\partial x_1} & \frac{\partial f_2}{\partial x_2} & \frac{\partial f_2}{\partial x_3} & \cdots & \frac{\partial f_2}{\partial x_n} \\ \frac{\partial f_3}{\partial x_1} & \frac{\partial f_3}{\partial x_2} & \frac{\partial f_3}{\partial x_3} & \cdots & \frac{\partial f_3}{\partial x_n} \\ \vdots & \vdots & \vdots & \ddots & \vdots \\ \frac{\partial f_n}{\partial x_1} & \frac{\partial f_n}{\partial x_2} & \frac{\partial f_n}{\partial x_3} & \cdots & \frac{\partial f_n}{\partial x_n} \end{bmatrix}\right|_{x=\hat{x}(t)} \tag{40}$$

where

$$f(x,t) = \dot{\boldsymbol{X}} = \bar{\mathrm{A}}\boldsymbol{X} + \mathrm{B}U \tag{41}$$

$$\{\boldsymbol{X}\} = [x_1, x_2, x_3, x_4, x_5, x_6, x_7, x_8]^T \tag{42}$$

and the Riccati equation for EKF is

$$\dot{P}_e(t) = F(t)P_e(t) + P_e(t)F(t) - P_e(t)\mathbf{C}^T R_e^{-1}\mathbf{C}P_e(t) + Q_e \tag{43}$$

also the EKF gain

$$K_e(t) = P_e(t)\mathbf{C}^T R_e^{-1} \tag{44}$$

The preceding equations indicate that the EKF gain is evaluated online.

IV. Results

A. Material Properties

The system equations of motion of the composite plate are transferred into modal equations. The time domain numerical method is employed to obtain the LCO. The fourth-order Runge–Kutta method [23] is used. Material properties of the composite plate, PZT5A, and MFC are shown in Table 1.

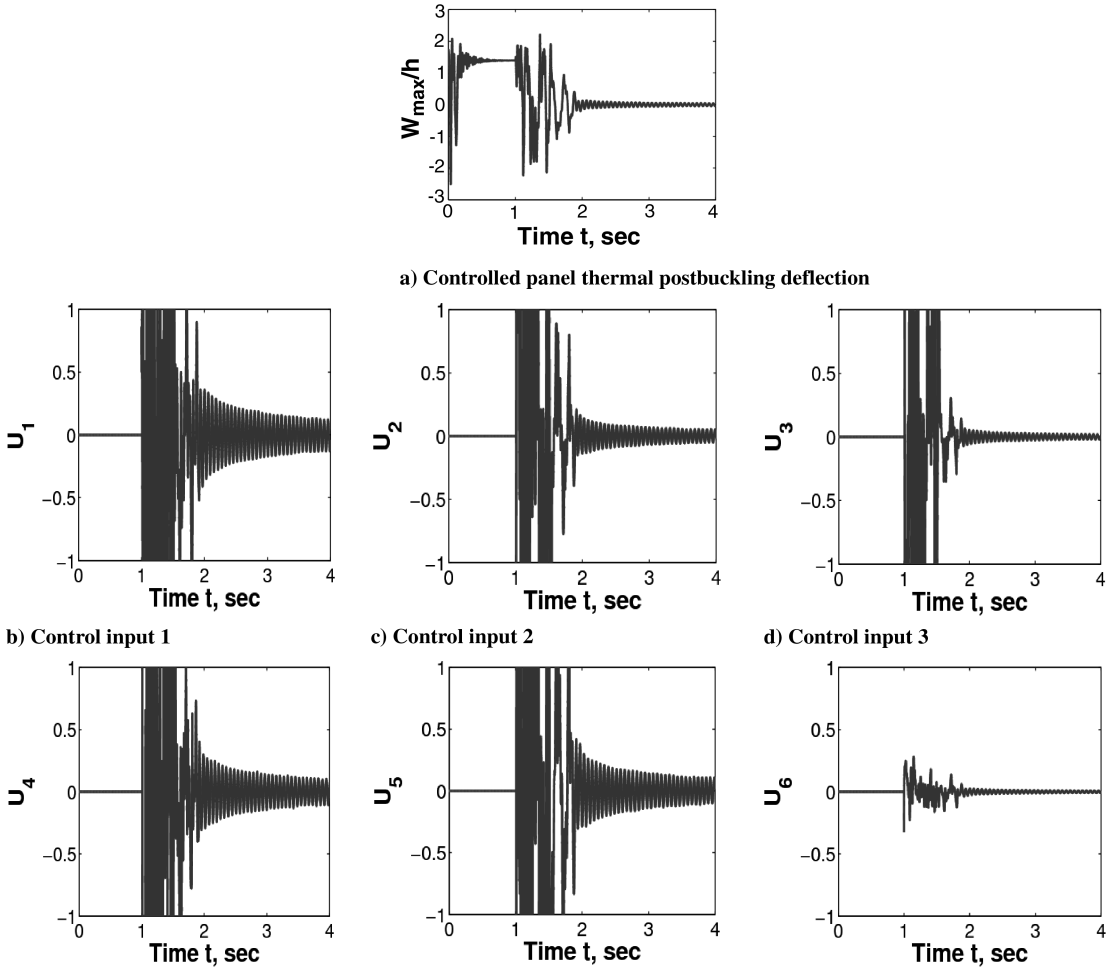

a) Controlled panel thermal postbuckling deflection

b) Control input 1 c) Control input 2 d) Control input 3

e) Control input 4 f) Control input 5 g) Control input 6

Fig. 7 Suppression of postbuckling deflection at $\lambda = 430$ and $\Delta T/\Delta T_{cr} = 8$ using PZT5A.

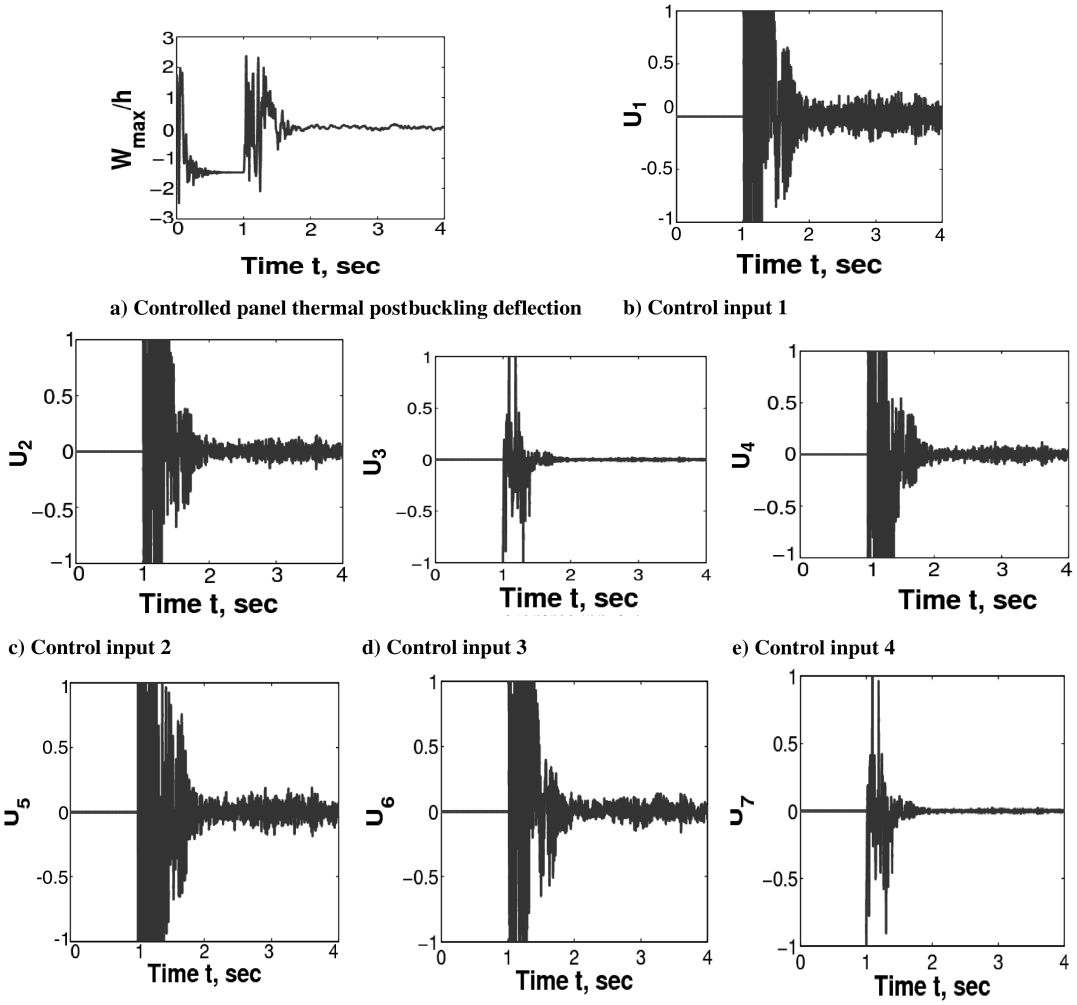

a) Controlled panel thermal postbuckling deflection b) Control input 1

c) Control input 2 d) Control input 3 e) Control input 4

f) Control input 5 g) Control input 6 h) Control input 7

Fig. 8 Suppression of postbuckling deflection at $\lambda = 430$ and $\Delta T/\Delta T_{cr} = 8$ using MFC.

B. Suppression of Panel Flutter

The model considered here is a symmetrically laminated six-layer [0 60 −60 −60 60 0 deg] rectangular panel. It is simply-supported on all four edges, and the in-plane boundary conditions are $u(0, y) = u(a, y) = v(x, 0) = v(x, b) = 0$. The dimensions of the panel are $102.87 \times 68.58 \times 0.1372$ cm ($40.5 \times 27 \times 0.054$ in.), and the finite element mesh has been chosen as 12×12 for the whole plate. This model is applied in all the flutter suppression with and without considering thermal loads.

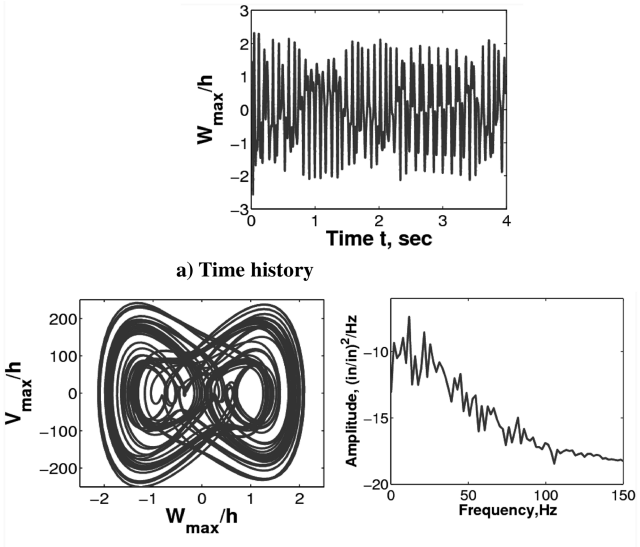

a) Time history

b) Phase plot c) Power spectrum density

Fig. 9 Chaotic response of the composite panel at $\lambda = 440$ and $\Delta T/\Delta T_{cr} = 8$ using 4 modes.

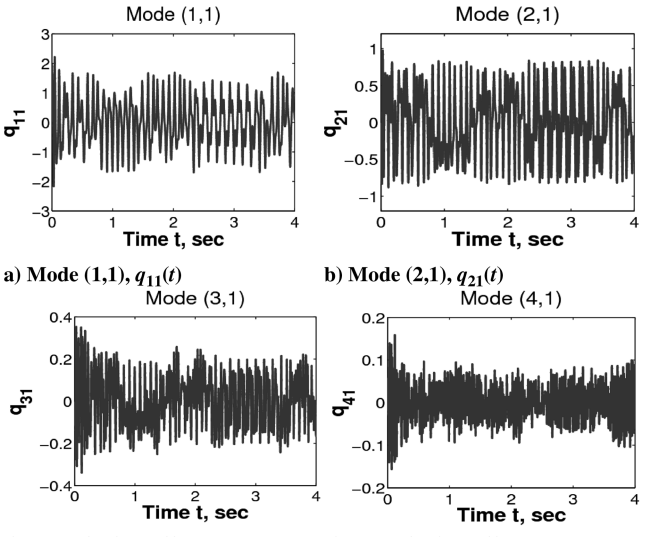

a) Mode (1,1), $q_{11}(t)$ b) Mode (2,1), $q_{21}(t)$

c) Mode (3,1), $q_{31}(t)$ d) Mode (4,1), $q_{41}(t)$

Fig. 10 Time histories of the 4 modes for the composite panel at $\lambda = 440$ and $\Delta T/\Delta T_{cr} = 8$.

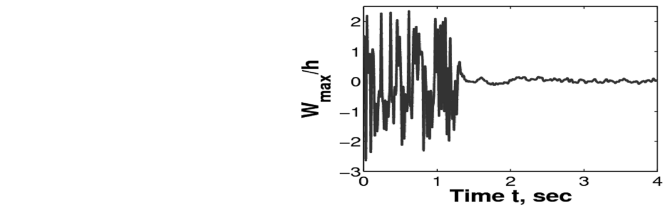

a) Controlled panel chaotic response

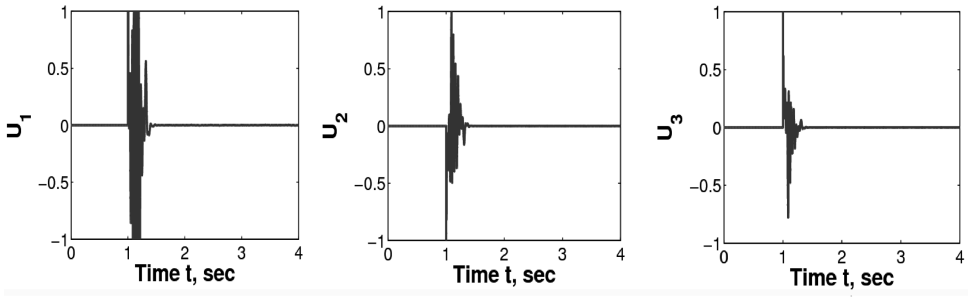

b) Control input 1 c) Control input 2 d) Control input 3

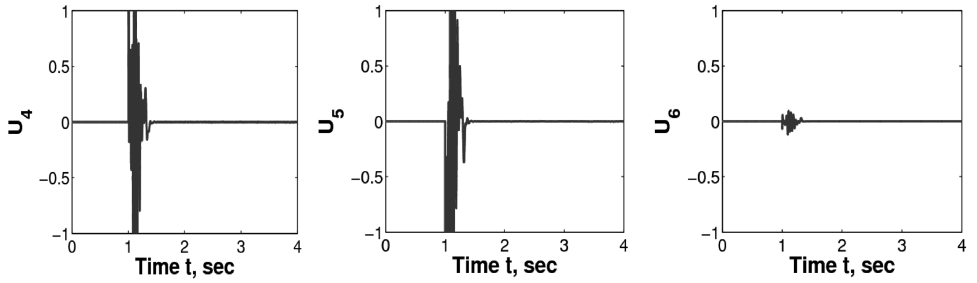

e) Control input 4 f) Control input 5 g) Control input 6

Fig. 11 Suppression of the chaotic response at $\lambda = 440$ and $\Delta T/\Delta T_{cr} = 8$ using PZT5A.

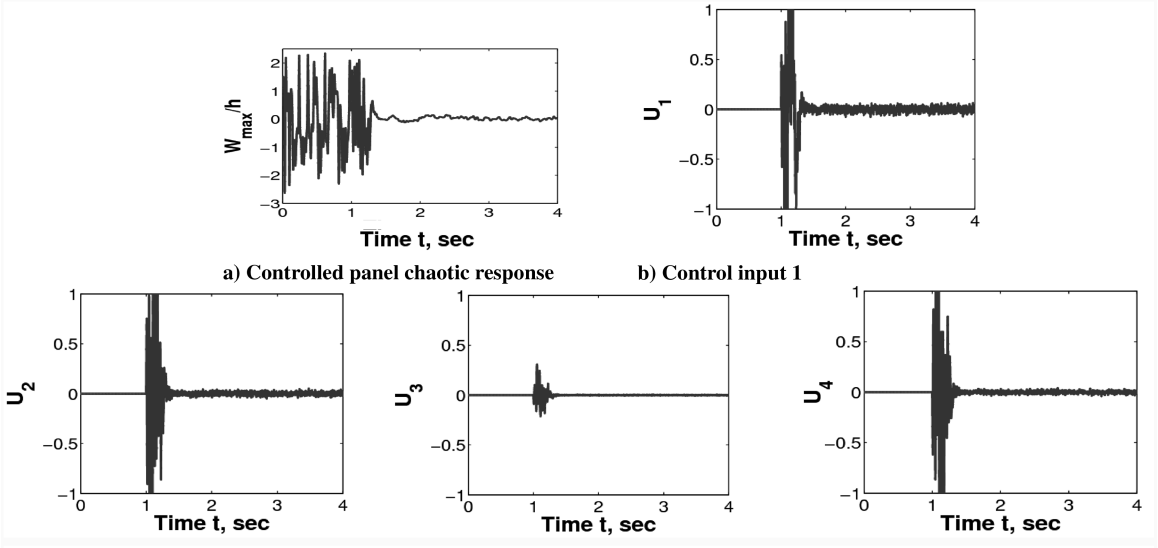

a) Controlled panel chaotic response b) Control input 1

c) Control input 2 d) Control input 3 e) Control input 4

f) Control input 5 g) Control input 6 h) Control input 7

Fig. 12 Suppression of the chaotic response at $\lambda = 440$ and $\Delta T/\Delta T_{cr} = 8$ using MFC.

1. Control of Panel Flutter Without Thermal Effects

When the thermal loads are not considered, the panel produces only LCO. Two piezoelectric materials: PZT5A and MFC are applied and compared in this paper. The NFCG and NKFEG methods are used to decide the locations for actuators and sensors. For PZT5A, the NFCG method is used to locate the actuators as shown in Fig. A1a. The NKFEG method is applied to place the sensors and the result is shown in Fig. A1b. The self-sensing actuators are placed at the optimal locations for both actuators and sensors, and Fig. A1c shows the final locations for the PZT5A case. The self-sensing actuators are embedded in the top and bottom surfaces of the composite panel using the NFCG norm >42.7 and NKFEG norm >0.0681. For MFC, because its stress constant is twice as large as that of PZT5A ($d_{11} > 2d_{31}$), MFC can provide more control force than PZT5A. Therefore, theoretically, MFC can provide better control performance than PZT5A. Figure A2 shows the optimal locations of MFC where the NFCG norm of the self-sensing actuators >42.9 and NKFEG norm >1.06. The results show that less actuators or sensors are needed in flutter suppression when using MFC.

11.1	11.4	13.3	3.07	27.4	11.7	3.72	2.51	5.68	5.97	38.3	8.74
10.6	10.7	11.9	3.91	16.4	10.6	5.22	2.32	6.58	4.34	23.3	29.8
10.4	10.2	11.5	4.96	16.5	10.2	5.54	2.97	6.34	4.61	24.5	16.8
10.2	9.45	11.4	5.43	4.71	10.2	5.7	3.85	5.87	4.41	12.7	5.96
10.1	9.72	10.9	5.25	4.75	10.1	5.68	4.24	5.88	4.18	3.29	2.61
9.98	9.99	10.4	5.05	4.61	10.2	5.86	4.45	6.3	5.27	11.4	2.63
9.69	9.89	10.8	5.27	4.25	10.4	6.03	4.09	7.61	8.18	54	3.75
9.99	10	11	5.25	4.52	10.8	6.35	4.2	8.25	8.96	28.3	4.52
9.95	10.3	10.8	4.66	4.84	11	6.5	3.83	8.95	7.31	20.8	3.49
9.72	10.6	10.9	4.77	4.83	11.8	6.76	3.97	14.2	18.9	37.5	3.96
9.46	10.7	11.8	4.91	4.97	13.6	6.61	4.86	29.9	43.3	42.7	9.87
6.02	9.96	12.1	3.75	5.37	24.8	6.7	7.77	42.9	22.4	25.9	865

a) NFCG norm of every element of the composite panel

1.52	1.5	1.06	5.65	1.25	4.6	1.97	1.16	0.705	3.72	6.76	2.5
0.021	0.676	0.672	1.1	0.16	0.33	0.144	0.141	0.065	0.322	0.474	0.07
0.0041	0.229	0.09	0.125	0.07	0.131	0.047	0.038	0.029	0.129	0.154	0.011
0.0025	0.002	0.01	0.029	0.005	0.091	0.02	0.018	0.018	0.08	0.083	0.005
0.0045	0.004	0.012	0.019	0.002	0.038	0.009	0.014	0.013	0.059	0.056	0.003
0.003	0.033	0.009	0.014	0.002	0.025	0.008	0.013	0.011	0.046	0.041	0.002
0.0014	0.06	0.003	0.008	0.001	0.021	0.006	0.019	0.011	0.036	0.034	0.002
0.0022	0.004	0.002	0.007	0.001	0.02	0.004	0.025	0.011	0.032	0.029	0.002
0.013	0.08	0.003	0.009	0.002	0.017	0.003	0.088	0.014	0.039	0.027	0.002
0.0367	0.12	0.011	0.015	0.004	0.024	0.004	0.217	0.028	0.063	0.051	0.003
0.0681	0.302	0.045	0.043	0.015	0.061	0.008	0.178	0.099	0.177	0.131	0.005
0.0333	1.76	0.305	0.577	0.205	0.932	0.103	1.99	1.44	2.36	1.63	0.039

b) NKFEG norm of every element of the composite panel

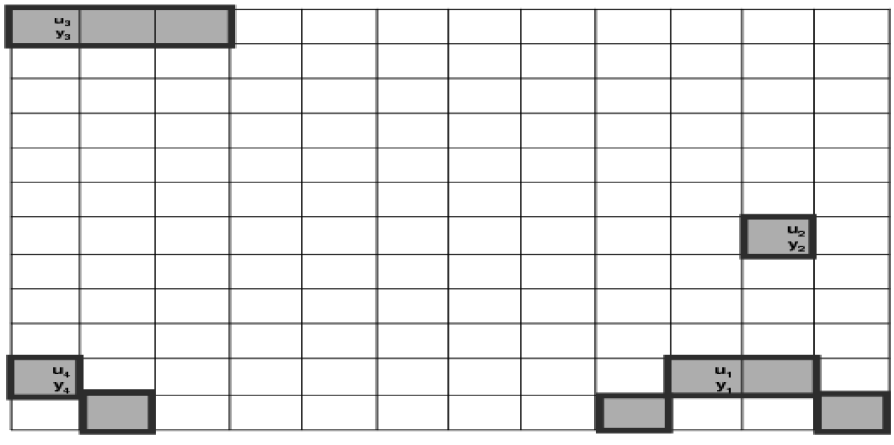

c) The optimal locations based on the two norms for the composite panel

Fig. A1 Optimal locations of PZT5A self-sensing actuator on the composite panel based on NFCG and NKFEG norm for LCO.

When the PZT5A actuators and sensors are placed on the three-dimensional composite panel using NFCG and NKFEG norms, the relationship of the dynamic pressure and $W_{\max}/h$ is shown in Fig. 1a. The time history, phase plot, and power spectrum density (PSD) plot at $\lambda = 700$ are shown in Figs. 1b–1d. Obviously, the motion is an LCO. The time histories of the four modes, $q_{11}(t)$, $q_{21}(t)$, $q_{31}(t)$, and $q_{41}(t)$ are shown in Fig. 2.

Figures 3 and 4 show the suppression of flutter by using PZT5A and MFC, respectively. From Figs. A1 and A2, it is noted that eight-element MFCs are used but ten-element PZT5As are needed to achieve the similar performance at a dynamic pressure $\lambda = 700$.

The results show that LQR/EFK can provide good control performance even if the initial state estimation is not accurate. That is because aerodynamic damping exists in the supersonic panel flutter and the damping will make the panel flutter converge to a particular LCO amplitude no matter what kind of initial states the system has. With this aerodynamic damping, the estimated states from EKF can converge to real states much faster than free vibration. Therefore, the

11.1	11.4	13.3	3.07	27.4	11.7	3.72	2.51	5.68	5.97	38.3	8.74
10.6	10.7	11.9	3.91	16.4	10.6	5.22	2.32	6.58	4.34	23.3	29.8
10.4	10.2	11.5	4.96	16.5	10.2	5.54	2.97	6.34	4.61	24.5	16.8
10.2	9.45	11.4	5.43	4.71	10.2	5.7	3.85	5.87	4.41	12.7	5.96
10.1	9.72	10.9	5.25	4.75	10.1	5.68	4.24	5.88	4.18	3.29	2.61
9.98	9.99	10.4	5.05	4.61	10.2	5.86	4.45	6.3	5.27	11.4	2.63
9.69	9.89	10.8	5.27	4.25	10.4	6.03	4.09	7.61	8.18	54	3.75
9.99	10	11	5.25	4.52	10.8	6.35	4.2	8.25	8.96	28.3	4.52
9.95	10.3	10.8	4.66	4.84	11	6.5	3.83	8.95	7.31	20.8	3.49
9.72	10.6	10.9	4.77	4.83	11.8	6.76	3.97	14.2	18.9	37.5	3.96
9.46	10.7	11.8	4.91	4.97	13.6	6.61	4.86	29.9	43.3	42.7	9.87
6.02	9.96	12.1	3.75	5.37	24.8	6.7	7.77	42.9	22.4	25.9	865

a) NFCG norm of every element of the composite panel

1.52	1.5	1.06	5.65	1.25	4.6	1.97	1.16	0.705	3.72	6.76	2.5
0.021	0.676	0.672	1.1	0.16	0.33	0.144	0.141	0.065	0.322	0.474	0.07
0.0041	0.229	0.09	0.125	0.07	0.131	0.047	0.038	0.029	0.129	0.154	0.011
0.0025	0.002	0.01	0.029	0.005	0.091	0.02	0.018	0.018	0.08	0.083	0.005
0.0045	0.004	0.012	0.019	0.002	0.038	0.009	0.014	0.013	0.059	0.056	0.003
0.003	0.033	0.009	0.014	0.002	0.025	0.008	0.013	0.011	0.046	0.041	0.002
0.0014	0.06	0.003	0.008	0.001	0.021	0.006	0.019	0.011	0.036	0.034	0.002
0.0022	0.004	0.002	0.007	0.001	0.02	0.004	0.025	0.011	0.032	0.029	0.002
0.013	0.08	0.003	0.009	0.002	0.017	0.003	0.088	0.014	0.039	0.027	0.002
0.0367	0.12	0.011	0.015	0.004	0.024	0.004	0.217	0.028	0.063	0.051	0.003
0.0681	0.302	0.045	0.043	0.015	0.061	0.008	0.178	0.099	0.177	0.131	0.005
0.0333	1.76	0.305	0.577	0.205	0.932	0.103	1.99	1.44	2.36	1.63	0.039

b) NKFEG norm of every element of the composite panel

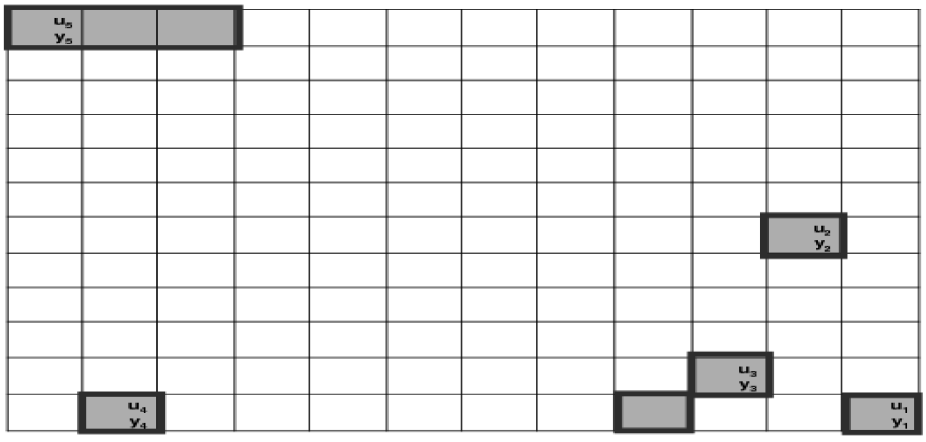

c) The optimal locations based on the two norms for the composite panel

Fig. A2 Optimal locations of MFC self-sensing actuator on the composite panel based on NFCG and NKFEG norm for LCO.

LQR/EKF controller has a good performance in the suppression of panel flutter of all cases (LCO, thermal postbuckling deflections, and chaotic motions).

2. *Control of Panel Flutter with Thermal Effects*

At elevated temperatures, flutter response could be one of the three: LCO (including periodic motions), thermal postbuckling deflections, and chaotic motions (e.g., see Fig. 2 of [1] or Fig. 1 of [18]). Most literatures studied the control of LCO without considering flutter suppression of the latter two cases. Because the suppression of LCO with thermal loads is similar to the situation without thermal effects, only static thermal postbuckling and chaotic cases will be presented in this section.

The presence of thermal loads results in a flutter LCO motion at lower dynamic pressure or a larger LCO amplitude at the same

11.1	11.4	13.3	3.07	27.4	11.7	3.72	2.51	5.68	5.97	38.3	8.74
10.6	10.7	11.9	3.91	16.4	10.6	5.22	2.32	6.58	4.34	23.3	29.8
10.4	10.2	11.5	4.96	16.5	10.2	5.54	2.97	6.34	4.61	24.5	16.8
10.2	9.45	11.4	5.43	4.71	10.2	5.7	3.85	5.87	4.41	12.7	5.96
10.1	9.72	10.9	5.25	4.75	10.1	5.68	4.24	5.88	4.18	3.29	2.61
9.98	9.99	10.4	5.05	4.61	10.2	5.86	4.45	6.3	5.27	11.4	2.63
9.69	9.89	10.8	5.27	4.25	10.4	6.03	4.09	7.61	8.18	54	3.75
9.99	10	11	5.25	4.52	10.8	6.35	4.2	8.25	8.96	28.3	4.52
9.95	10.3	10.8	4.66	4.84	11	6.5	3.83	8.95	7.31	20.8	3.49
9.72	10.6	10.9	4.77	4.83	11.8	6.76	3.97	14.2	18.9	37.5	3.96
9.46	10.7	11.8	4.91	4.97	13.6	6.61	4.86	29.9	43.3	42.7	9.87
6.02	9.96	12.1	3.75	5.37	24.8	6.7	7.77	42.9	22.4	25.9	865

a) NFCG norm of every element of the composite panel

1.52	1.5	1.06	5.65	1.25	4.6	1.97	1.16	0.705	3.72	6.76	2.5
0.021	0.676	0.672	1.1	0.16	0.33	0.144	0.141	0.065	0.322	0.474	0.07
0.0041	0.229	0.09	0.125	0.07	0.131	0.047	0.038	0.029	0.129	0.154	0.011
0.0025	0.002	0.01	0.029	0.005	0.091	0.02	0.018	0.018	0.08	0.083	0.005
0.0045	0.004	0.012	0.019	0.002	0.038	0.009	0.014	0.013	0.059	0.056	0.003
0.003	0.033	0.009	0.014	0.002	0.025	0.008	0.013	0.011	0.046	0.041	0.002
0.0014	0.06	0.003	0.008	0.001	0.021	0.006	0.019	0.011	0.036	0.034	0.002
0.0022	0.004	0.002	0.007	0.001	0.02	0.004	0.025	0.011	0.032	0.029	0.002
0.013	0.08	0.003	0.009	0.002	0.017	0.003	0.088	0.014	0.039	0.027	0.002
0.0367	0.12	0.011	0.015	0.004	0.024	0.004	0.217	0.028	0.063	0.051	0.003
0.0681	0.302	0.045	0.043	0.015	0.061	0.008	0.178	0.099	0.177	0.131	0.005
0.0333	1.76	0.305	0.577	0.205	0.932	0.103	1.99	1.44	2.36	1.63	0.039

b) NFFEG norm of every element of the composite panel

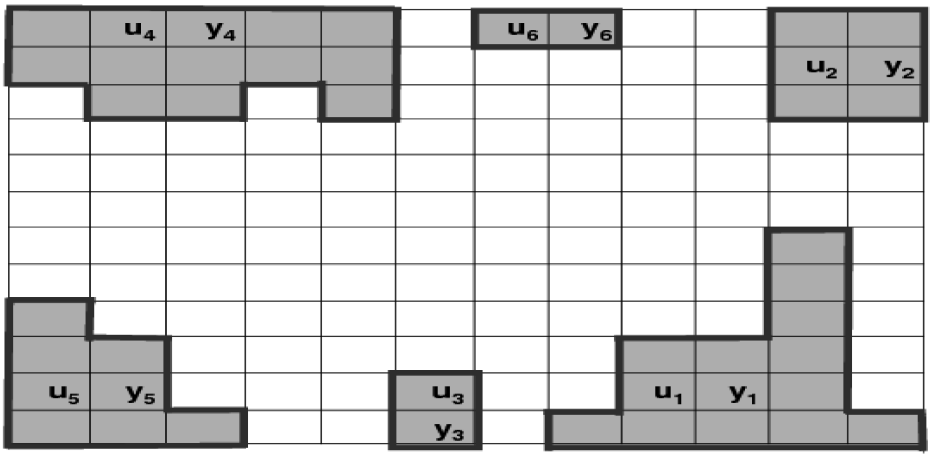

c) The optimal locations based on the two norms for the composite panel

Fig. A3 Optimal locations of PZT5A self-sensing actuator on the composite panel based on NFCG and NKFEG norm for static thermal postbuckling and chaotic motion.

dynamic pressure. In addition, a high temperature rise may cause large thermal postbuckling deflections of the skin panels, which could lead to chaotic motions at a certain range of dynamic pressure. More self-sensing actuators are needed to suppress such static postbuckling deflections or chaotic motions. It is also noted that the state estimator plays an important role in the control. Sometimes, fewer actuators are enough to achieve the suppression, but a lot more sensors are needed to supply the state information for the controller. And so, additional sensors may be needed besides the self-sensing actuators.

First, the suppression of thermal postbuckling deflection is considered. The thermal load to this three-dimensional composite panel is eight times the critical temperature, $\Delta T/\Delta T_{\text{cr}} = 8$. The dynamic pressure is at $\lambda = 430$, which is less than the critical dynamic pressure in LCO case. And from the time history shown in Fig. 5, the panel produces a large static thermal postbuckling

11.1	11.4	13.3	3.07	27.4	11.7	3.72	2.51	5.68	5.97	38.3	8.74
10.6	10.7	11.9	3.91	16.4	10.6	5.22	2.32	6.58	4.34	23.3	29.8
10.4	10.2	11.5	4.96	16.5	10.2	5.54	2.97	6.34	4.61	24.5	16.8
10.2	9.45	11.4	5.43	4.71	10.2	5.7	3.85	5.87	4.41	12.7	5.96
10.1	9.72	10.9	5.25	4.75	10.1	5.68	4.24	5.88	4.18	3.29	2.61
9.98	9.99	10.4	5.05	4.61	10.2	5.86	4.45	6.3	5.27	11.4	2.63
9.69	9.89	10.8	5.27	4.25	10.4	6.03	4.09	7.61	8.18	54	3.75
9.99	10	11	5.25	4.52	10.8	6.35	4.2	8.25	8.96	28.3	4.52
9.95	10.3	10.8	4.66	4.84	11	6.5	3.83	8.95	7.31	20.8	3.49
9.72	10.6	10.9	4.77	4.83	11.8	6.76	3.97	14.2	18.9	37.5	3.96
9.46	10.7	11.8	4.91	4.97	13.6	6.61	4.86	29.9	43.3	42.7	9.87
6.02	9.96	12.1	3.75	5.37	24.8	6.7	7.77	42.9	22.4	25.9	865

a) NFCG norm of every element of the composite panel

1.52	1.5	1.06	5.65	1.25	4.6	1.97	1.16	0.705	3.72	6.76	2.5
0.021	0.676	0.672	1.1	0.16	0.33	0.144	0.141	0.065	0.322	0.474	0.07
0.0041	0.229	0.09	0.125	0.07	0.131	0.047	0.038	0.029	0.129	0.154	0.011
0.0025	0.002	0.01	0.029	0.005	0.091	0.02	0.018	0.018	0.08	0.083	0.005
0.0045	0.004	0.012	0.019	0.002	0.038	0.009	0.014	0.013	0.059	0.056	0.003
0.003	0.033	0.009	0.014	0.002	0.025	0.008	0.013	0.011	0.046	0.041	0.002
0.0014	0.06	0.003	0.008	0.001	0.021	0.006	0.019	0.011	0.036	0.034	0.002
0.0022	0.004	0.002	0.007	0.001	0.02	0.004	0.025	0.011	0.032	0.029	0.002
0.013	0.08	0.003	0.009	0.002	0.017	0.003	0.088	0.014	0.039	0.027	0.002
0.0367	0.12	0.011	0.015	0.004	0.024	0.004	0.217	0.028	0.063	0.051	0.003
0.0681	0.302	0.045	0.043	0.015	0.061	0.008	0.178	0.099	0.177	0.131	0.005
0.0333	1.76	0.305	0.577	0.205	0.932	0.103	1.99	1.44	2.36	1.63	0.039

b) NKFEG norm of every element of the composite panel

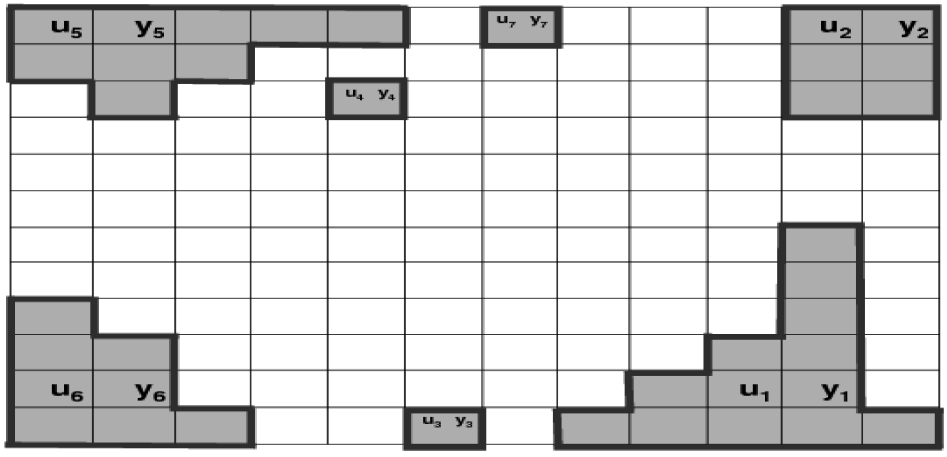

c) The optimal locations based on the two norms for the composite panel

Fig. A4 Optimal locations of MFC self-sensing actuator on the composite panel based on NFCG and NKFEG norm for static thermal postbuckling and chaotic motion.

deflection response. The locations of actuators and sensors from the NFCG and NKFEG methods are shown in Figs. A3 and A4 for PZT5A and MFC, respectively.

Figures 5 and 6 show the thermal postbuckling response with PZT5A embedded symmetrically in the top and bottom layers of the composite panel. The control results are shown in Figs. 7 and 8 for PZT5A and MFC, respectively. More self-sensing actuators are applied to suppress thermal deflection than the LCO case. The results also show that MFC is more efficient.

Second, the suppression of chaotic motions is studied. The thermal load to this three-dimensional composite panel is eight times the critical temperature. The dynamic pressure $\lambda = 440$, which is less than the critical dynamic pressure in the LCO case, and the panel produces large amplitude chaotic motion. Locations of actuators/sensors are the same as those for the static thermal postbuckling suppression.

Figure 9 shows the chaotic response of the maximum deflection of the composite panel in time history, phase plot, and PSD plot. Comparing to the corresponding plots for the LCO shown in Fig. 1, it clearly indicates that the motion at $\lambda = 440$ and $\Delta T/\Delta T_{cr} = 8$ is chaos. The time histories from the four modes are shown in Fig. 10. The control results are shown in Figs. 11 and 12 for PZT5A and MFC, respectively.

V. Conclusions

Suppression of the nonlinear panel flutter with or without thermal effects for a three-dimensional composite panel by using the linear quadratic regulator with extended kalman filter is studied. When there are no thermal loads, limit cycle oscillations are observed. The fundamental mode contributes more than 50% to the LCO response, and the contributions from other modes need also to be considered. Therefore, more control efforts and sensors are needed for the flutter suppression. But aerodynamic damping will make panel response converge to some particular motions no matter what initial states it has, and it also makes the estimated states from EKF converge to the real states much faster than the case for the suppression of free vibration [9].

When there exists thermal loads, the panels become less stiff and may generate thermal postbuckling deflection, limit cycle oscillations (including periodic motions), and chaotic motions. Numerical simulations showed that the LQR/EKF can suppress the panel motions with proper selection for sensor/actuator locations. The piezoelectric MFC is more efficient than PZT5A. Sensors used for EKF also play a more important roll in the overall control performance. The present investigations have shown for the first time that all three panel responses (LCO, thermal postbuckling, and chaos) can be suppressed. When the flow angle, dynamic pressure, and thermal loads are changing, the panel motion may vary among the static postbuckling, LCO, periodic, and chaotic motions. In this case, an adaptive or other intelligent controller will be needed for future studies.

Appendix: Placement of Self-Sensing Actuators

References

[1] Mei, C., Abdel-Motagaly, K., and Chen, R., "Review of Nonlinear Panel Flutter at Supersonic and Hypersonic Speeds," *Applied Mechanics Reviews*, Vol. 52, No. 10, 1999, pp. 321–332.

[2] Zhou, R. C., Lai, Z. H., Xue, D. Y., Huang, J. K., and Mei, C., "Suppression of Nonlinear Panel Flutter with Piezoelectric Actuators Using Finite Element Method," *AIAA Journal*, Vol. 33, No. 6, 1995, pp. 1098–1105.

[3] Zhou, R. C., Mei, C., and Huang, J. K., "Suppression of Nonlinear Panel Flutter at Supersonic Speeds and Elevated Temperatures," *AIAA Journal*, Vol. 34, No. 2, 1996, pp. 347–354.

[4] Moon, S. H., and Kim, S. J., "Suppression of Nonlinear Composite Panel Flutter with Active/Passive Hybrid Piezoelectric Networks Using Finite Element Methods," *Computers and Structures*, Vol. 59, No. 4, 2003, pp. 525–533.

[5] Park, J. S., and Kim, J. H., "Suppression of Aero-Thermal Large Deflections and Snap-Through Behaviors of Composite Panels Using Macro Fiber Composite Actuators," *Smart Materials and Structures*, Vol. 13, No. 6, 2004, pp. 448–1459.

[6] Wilkie, W. K., Bryant, R. G., High, J. W., Fox, R. L., Hellbaum, R. F., Jalink, A., Little, B. D., and Mirick, P. H., "Low-Cost Piezocomposite Actuator for Structural Control Application," *Proceedings of SPIE, 7th International Symposium on Smart Structures and Materials, Newport Beach, CA*, Vol. 3991, Society of Photo-Optical Instrumentation Engineers, 2000, pp. 323–334.

[7] Azzouz, M. S., Mei, C., Bevan, J. S., and Ro, J. J., "Finite Element Modeling of MFC/AFC Actuators and Performance of MFC," *Journal of Intelligent Material Systems and Structures*, Vol. 12, Sept. 2001, pp. 601–612.

[8] Moon, S. H., Chwa, D., and Kim, S. J., "Feedback Linearization Control for Panel Flutter Suppression with Piezoelectric Actuators," *AIAA Journal*, Vol. 43, No. 9, Sept. 2005, pp. 2069–2072.

[9] Li, Q., Phairoh, T., Huang, J. K., and Mei, C., "Adaptive Control of Nonlinear Free Vibrations of Composite Plates Using Piezoelectric Actuators," *AIAA Journal*, Vol. 44, No. 6, June 2006, pp. 1169–1180.

[10] Friedland, B., *Control System Design*, McGraw–Hill, New York, 1986.

[11] Stengel, F. R., *Stochastic Optimal Control*, Wiley, New York, 1986.

[12] Dowell, E. H., "Panel Flutter: A Review of the Aeroelastic Stability of Plates and Shells," *AIAA Journal*, Vol. 8, No. 3, 1970, pp. 385–399.

[13] Dowell, E. H., "Nonlinear Oscillations of a Fluttering Plate 1," *AIAA Journal*, Vol. 4, July 1966, pp. 1267–1275.

[14] Houbolt, J. C., "Study of Several Aerothermoelastic Problems of Aircraft in High Speed Flight," Ph.D. Thesis, Mitteilung aus dem Inst. fur Flugzeugstatikund Leichtbau, Nr 5, Swiss Federal Inst. of Technology (ETH), Zurich 1958.

[15] Mei, C., "Finite Element Approach for Nonlinear Panel Flutter," *AIAA Journal*, Vol. 15, No. 8, 1977, pp. 1107–1110.

[16] von Karman, "Festigkeitsprobleme im maschinenbau," *Encyklopaedie der Mathematischen Wissenschaften IV*, Teubner, Leipzig, Germany, 1910.

[17] Bogner, F. K., Fox, R. L., and Schmit, L. A., "Generation of Inter-Element Compatible Stiffness and Mass Matrices by the Use of Interpolation Formulas," Air Force Flight Dynamics Lab. No. TR-66-80, Wright-–Patterson AFB, OH, 1966, pp. 397–443.

[18] Zhou, R. C., Xue, D. Y., and Mei, C., "Finite Element Time Domain: Modal Formulation for Nonlinear Flutter of Composite Panels," *AIAA Journal*, Vol. 32, No. 10, 1994, pp. 2044–2052.

[19] Cheng, G., Lee, Y. Y., and Mei, C., "Flow Angle, Temperature, and Aerodynamic Damping on Supersonic Panel Flutter Stability Boundary," *Journal of Aircraft*, Vol. 40, No. 2, 2003, pp. 248–255.

[20] Abdel-Motagaly, K., Guo, X., Duan, B., and Mei, C., "Active Control of Nonlinear Panel Flutter Under Yawed Supersonic Flow," *AIAA Journal*, Vol. 43, No. 3, 2005, pp. 671–680.

[21] Abdel-Motagaly, K., "Finite Element Analysis and Active Control for Nonlinear Flutter of Composite Panes Under Yawed Supersonic Flow," Ph.D. Thesis, Dept. of Aerospace Engineering, Old Dominion Univ., Norfolk, VA, Dec. 2001.

[22] Grewal, M. S., and Andrews, A. P., *Kalman Filtering: Theory and Practice Using MATLAB*, 2nd ed., Wiley, New York, 2001, Chap. 5, pp. 175–184.

[23] Dormand, J. R., and Prince, P. J., "Family of Embedded Runge-Kutta Formulae," *Journal of Computational and Applied Mathematics*, Vol. 6, No. 1, 1980, pp. 19–26.

A. Palazotto
Associate Editor